Acta Astronautica Vol. 12, No. 1, pp. 11–25, 1985
Printed in Great Britain

0094–5765/85 $3.00 + .00
Pergamon Press Ltd.

OPTIMAL AEROASSISTED RETURN FROM HIGH EARTH ORBIT WITH PLANE CHANGE†

NGUYEN X. VINH
Department of Aerospace Engineering, The University of Michigan, Ann Arbor, MI 48109-2140, U.S.A.

and

JOHN M. HANSON
Analytic Services, Inc., Arlington, VA 22202, U.S.A.

(*Received* 31 *January* 1984)

Abstract—This paper gives a complete analysis of the problem of aeroassisted return from a high Earth orbit to a low Earth orbit with plane change. A discussion of pure propulsive maneuver leads to the necessary change for improvement of the fuel consumption by inserting in the middle of the trajectory an atmospheric phase to obtain all or part of the required plane change. The variational problem is reduced to a parametric optimization problem by using the known results in optimal impulsive transfer and solving the atmospheric turning problem for storage and use in the optimization process. The coupling effect between space maneuver and atmospheric maneuver is discussed. Depending on the values of the plane change i, the ratios of the radii, $n = r_1/r_2$ between the orbits and $\alpha = r_2/R$ between the low orbit and the atmosphere, and the maximum lift-to-drag ratio E^* of the vehicle, the optimal maneuver can be pure propulsive or aeroassisted. For aeroassisted maneuver, the optimal mode can be parabolic, which requires only drag capability of the vehicle, or elliptic. In the elliptic mode, it can be by one-impulse for deorbit and one or two-impulse in postatmospheric flight, or by two-impulse for deorbit with only one impulse for final circularization. It is shown that whenever an impulse is applied, a plane change is made. The necessary conditions for the optimal split of the plane changes are derived and mechanized in a program routine for obtaining the solution.

1. INTRODUCTION

It has been known since the pioneering work by London[1] that the use of aerodynamic forces to assist in the orbital transfer can significantly reduce the fuel consumption as compared to the pure propulsive mode. For the classical analyses, we refer to the monograph by Vinh[2] and the recent review by Walberg[3]. In the published literature, when atmospheric flight is involved, the aerodynamic vehicle, referred to as the Orbital Transfer Vehicle (OTV), is always considered in the form of a particular flying apparatus with a set of specified physical parameters. These restrictions prevent any generalization of the fine results obtained. Furthermore, there is always a mathematical difficulty for a smooth transition from atmospheric dynamics to space dynamics in the vacuum due to different preferences in the selection of the appropriate coordinate systems for describing these two phases. As a consequence, not much effort has been done to analyze the coupling effect between space maneuver and atmospheric maneuver and its subsequent influence on the performance index, which is here the total characteristic velocity for the combined propulsive atmospheric maneuver. As an illustration of the fact that orbital flight and high altitude atmospheric flight at hypersonic speeds can be considered as an integral problem in astrodynamics under a global optimization to find the combined optimal trajectory for the OTV, we consider the problem of minimum-fuel aeroassisted return from a high Earth orbit (HEO), with radius r_1, to a low Earth orbit (LEO), with radius r_2, with occasional maneuvers inside an atmosphere with radius R, while performing a plane change of an angle i.

2. OPTIMAL PLANAR RETURN

We first consider the case of aeroassisted planar return from HEO to LEO, with no plane change, $i = 0$, and then see how the optimal strategy can be modified to also perform a plane change.

The different transfers are shown in Fig. 1, and the analysis depends on the ratios of the radii

$$n = \frac{r_1}{r_2}, \qquad \alpha = \frac{r_2}{R}. \tag{1}$$

We use the circular speed at LEO as unit speed and calculate the dimensionless velocities

$$v = \frac{V}{\sqrt{\mu/r_2}}, \qquad \Delta v_i = \frac{\Delta V_i}{\sqrt{\mu/r_2}}, \tag{2}$$

where μ is the gravitational constant. For pure propulsive maneuver, the optimal mode is either the Hohmann transfer with characteristic velocity

$$\Delta v_H = \frac{1}{\sqrt{n}} - 1 + (n - 1)\sqrt{\frac{2}{n(n+1)}} \tag{3}$$

†Paper presented at the 34th Congress of the International Astronautical Federation, Budapest, Hungary, 10–15 October 1983.

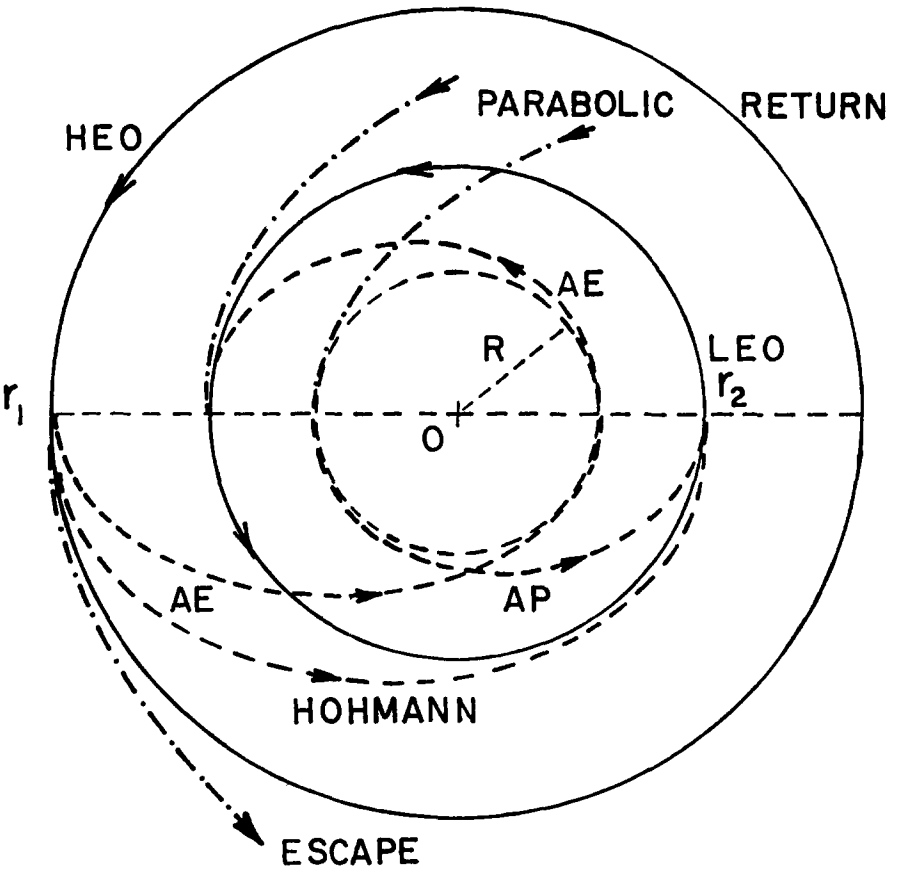

Fig. 1. Planar return from HEO to LEO.

or the parabolic mode with characteristic velocity

$$\Delta v_P = (\sqrt{2} - 1)\left(1 + \frac{1}{\sqrt{n}}\right). \tag{4}$$

In the parabolic mode, the vehicle will go parabolic from HEO to infinity and then return via another parabola for circularization at LEO. The parabolic transfer is more economical than the Hohmann transfer when $n >$ 11.938765.

For aeroassisted maneuver, we can apply tangentially a decelerating impulse at HEO to send the OTV along a descending elliptic trajectory for grazing the atmosphere at the distance R. At this perigee, atmospheric drag will work to reduce the apogee from HEO to LEO for circularization. The total characteristic velocity for this aeroassisted-elliptic mode is

$$\Delta v_{AE} = \frac{1}{\sqrt{n}}\left[1 - \sqrt{\frac{2}{n\alpha + 1}}\right] + 1 - \sqrt{\frac{2}{\alpha + 1}}. \tag{5}$$

Another way for achieving a grazing trajectory is to first send the OTV from HEO into a parabola and then return without fuel consumption from infinity along a grazing parabola. The total characteristic velocity for this aeroassisted-parabolic mode, including a final cost for circularization at LEO is

$$\Delta v_{AP} = \frac{(\sqrt{2} - 1)}{\sqrt{n}} + 1 - \sqrt{\frac{2}{\alpha + 1}}. \tag{6}$$

The process of reducing the apogee through atmospheric drag acting at perigee, at distance R, requires several passages, but the work done by Cruz and his group at the Jet Propulsion Laboratory[4] has shown that the reduction can be achieved in one pass without significant increase in fuel consumption.

Upon comparison between these modes, we have the results shown in Fig. 2. In particular, the AP mode is better than the P mode when $\alpha < 2(\sqrt{2} + 1)$. Later on in the analysis, we shall consider the ratio α_1 between the HEO radius and the radius of the atmosphere. Hence we define

$$\alpha_1 = \frac{r_1}{R}, \qquad \text{or } n\alpha = \alpha_1. \tag{7}$$

For a geosynchronous orbit (GEO), taking $r_1 = 42,164$ km, $R = 6498$ km, we have $\alpha_1 = 6.4888$. The line representing a GEO, $n\alpha = 6.4888$, which is a hyperbola in the (n, α) space, is plotted in the dashed line in Fig. 2 and it is entirely in the AP region up to a value $\alpha = 1.99$, hence up to a very high LEO.

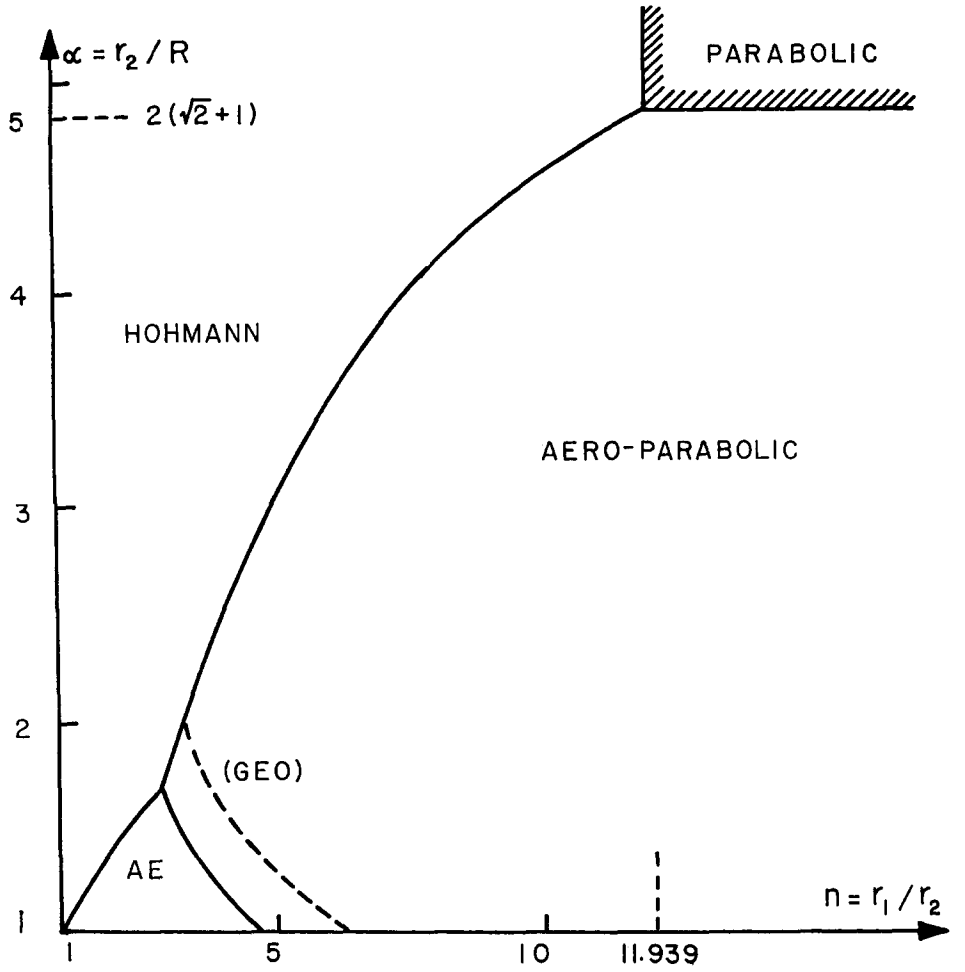

Fig. 2. Regions of optimality for planar return.

Figure 2 represents the section $i = 0$, for planar return, in the global assessment of optimality for the problem of return with plane change in the three-dimensional (n, a, i) space. Before achieving that in the next section, when we consider all the subspaces, i = constant, one pertinent remark is in order. For $i \neq 0$, the Hohmann transfer becomes the two- or three-impulse mode, and the characteristic velocity increases as the plane change angle increases. On the other hand, when the optimal mode involves a parabola, the fuel consumption, for any prescribed n and a, remains the same as for the planar case since the plane rotation can be achieved without cost at infinity. Hence, if the P or AP mode is optimal in the planar case, it remains optimal, with the same cost for any plane change. As a consequence, when a LEO is such that $a = r_2/R \leq 1.99$, the optimal return from GEO, for any plane change, is through the AP mode and the process only requires drag capability of the vehicle.

3. OPTIMAL RETURN WITH PLANE CHANGE

We now consider the optimal return with a prescribed plane change i and construct the different regions of optimality in the (n, a) subspace. As noticed above, the P and AP sets in the section $i = 0$ are both minimal sets. As the plane change i increases, they increase at the expense of the Hohmann set.

From the work of Marchal[5], it is known that when $i \neq 0$, the Hohmann transfer becomes a two- or three-impulse transfer, which must be compared with the parabolic transfer. The results are summarized in Fig. 3.

A two-impulse transfer is achieved via a generalized Hohmann transfer orbit connecting HEO to LEO with plane changes i_1 and i_2. The impulses are applied orthogonally to the position vectors and at the angles δ_1 and δ_2 with respect to the plane of the transfer orbit. The solution is obtained by solving the system

$$\frac{\sin(\delta_1 + i_1)}{\sin \delta_1} = \sqrt{\frac{2}{n+1}},$$

$$\frac{\sin(\delta_2 + i_2)}{\sin \delta_2} = \sqrt{\frac{2n}{n+1}} \tag{8}$$

$$\sin \delta_1 + n \sin \delta_2 = 0, \qquad i_1 + i_2 = i.$$

From this, we compute the characteristic velocities

$$\Delta v_1 = \frac{\sin i_1}{\sqrt{n}\sin\delta_1}, \qquad \Delta v_2 = -\frac{\sin i_2}{\sin\delta_2}. \tag{9}$$

In the three-impulse scheme, the impulses are also orthogonal to the position vectors with successive plane changes i_1, i_2 and i_3. The first impulse is designed to make the plane change i_1 and at the same time propel the OTV into a higher orbit with apogee at distance $r_1 x$. At this point, the second impulse is applied for a plane change i_2 and a reduction of perigee to the LEO level, at distance r_2. The third impulse circularizes the orbit with the last plane change i_3. If we use the plane of the first transfer orbit as reference plane to measure the thrust angle δ_1 and δ_2, and the plane of the second transfer orbit as reference plane to measure the thrust angle δ_3, then the solution is obtained by solving the system

$$\begin{aligned}
&\frac{\sin(\delta_1 + i_1)}{\sin\delta_1} = \sqrt{\frac{2x}{x+1}},\\
&\frac{\sin(\delta_2 + i_2)}{\sin\delta_2} = \sqrt{\frac{nx+1}{x+1}}\\
&\frac{\sin(\delta_3 - i_3)}{\sin\delta_3} = \sqrt{\frac{2nx}{nx+1}}\\
&x\sin\delta_1 + \sin\delta_2 = 0,\\
&nx\sin\delta_3 + \sin(\delta_2 + i_2) = 0,\\
&i_1 + i_2 + i_3 = i,\\
&\frac{(2nx+1)\sin i_2}{x(nx+1)\sin\delta_2} - \frac{n\cos\delta_3}{(nx+1)} + \frac{\sqrt{nx+1}\cos\delta_1}{(x+1)\sqrt{x+1}}\\
&\qquad - \frac{(n-1)\cos\delta_2}{(x+1)\sqrt{(x+1)(nx+1)}} = 0.
\end{aligned} \tag{10}$$

From this, we obtain the magnitudes of the impulses

$$\begin{aligned}
\Delta v_1 &= \frac{\sin i_1}{\sqrt{n}\sin\delta_1},\\
\Delta v_2 &= -\frac{\sin i_2}{\sin\delta_2}\sqrt{\frac{2}{nx(nx+1)}},\\
\Delta v_3 &= \frac{\sin i_3}{\sin\delta_3}.
\end{aligned} \tag{11}$$

The two finite-time transfers have to be compared with the parabolic mode which consists of sending the vehicle into escape for plane rotation at infinity without cost and return to LEO for circularization. On the other hand, the two-impulse transfer is the limit of the three-impulse transfer when $x \to 1$. This leads us to obtain the parametric equations for the separatrix between two and three-impulse regions as shown in Fig. 3. Let

$$k = \sqrt{3(2n+1)}. \tag{12}$$

After extensive algebraic manipulation, we have the explicit solution for the two-impulse transfer along the separatrix.

$$\begin{aligned}
\cos\delta_1 &= -\frac{1}{6}\sqrt{\frac{(k-3)^3}{(k-1)}},\\
\cos\delta_2 &= -\frac{k(k+1)}{6n}\sqrt{\frac{(k-3)}{(k-1)}}.
\end{aligned} \tag{13}$$

For each prescribed n, we compute the thrust angles and easily deduce i_1 and i_2 from eqns (8). Their sum gives the limiting plane change angle i, beyond which the three-impulse transfer is more economical. At this limit, we have for the characteristic velocities in explicit form

$$\begin{aligned}
\Delta v_1 &= \frac{(k+3)}{6}\sqrt{\frac{2(k-3)}{n(n+1)(k-1)}}\\
\Delta v_2 &= \frac{1}{6}\\
&\quad\times\sqrt{\frac{2(k-3)}{n(n+1)(k-1)}}\left[k(k+1)\right.\\
&\quad\left.-\sqrt{\frac{1}{2}(k^4+2k^3+8k^2+6k-9)}\right].
\end{aligned} \tag{14}$$

By setting their sum equal to the cost for parabolic mode, as given in eqn (4), we have the equation for calculating the value n where the three modes are equal. This point, shown in Fig. 3, is now known accurately to be

$$\begin{aligned}
n &= 6.67347605\\
i &= 37°389301.
\end{aligned} \tag{15}$$

In the figure, the limiting points on the axes are also accurately known as $n = 11.938765$ and $i = 60°1848448$.

Figure 4 shows the different regions of optimality for the case of $i = 30°$. In the section i = constant, the P and AP modes are always equal at $\alpha = 2(\sqrt{2}+1)$. The comparison between the H mode and the AP mode is straightforward. For any prescribed value i, the H mode, which can be a two- or a three-impulse mode, depends on the value of n, as determined by the explicit analysis described above. Once its characteristic velocity has been computed using these equations (which have been derived using the theory of the primer vector[6]), it can be compared with the characteristic velocity for the AP mode as given in eqn (6) as a function of the two parameters n and α. The limiting curve can then be generated in the (n, α) space.

For $i \neq 0$, the AE mode requires lifting capability of the vehicle. As shown in the next section, the only vehicle parameter involved in the analysis is the maximum lift-to-drag ratio E^* which is taken as $E^* = 1.5$ for the computation in the present analysis. To perform the AE transfer, we first use a deorbiting scheme, with or without plane change and by one or two impulses to enter the atmosphere at a small angle γ_e and speed V_e. The optimal atmospheric turning yields a maximum plane

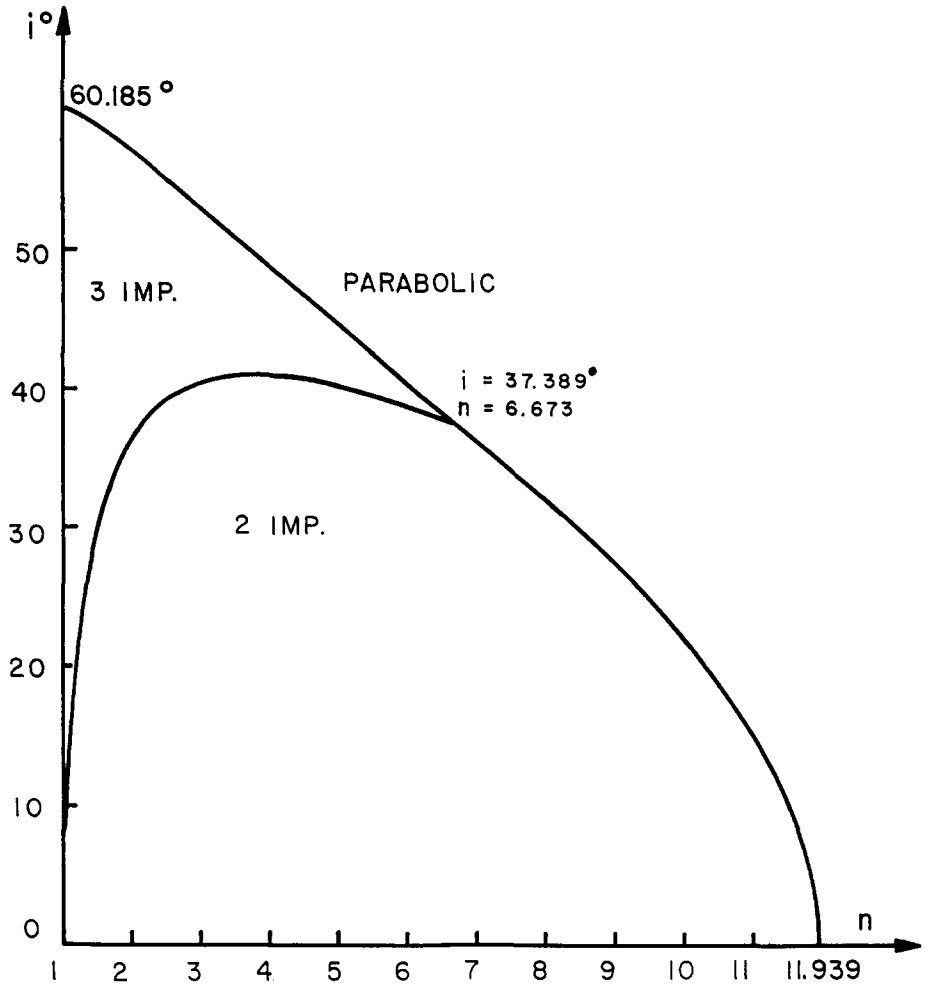

Fig. 3. Optimal pure propulsive modes.

change and an exit at a shallow angle with residual speed V_f necessary for an ascent to apogee at LEO for circularization. If this maximum plane change exceeds the prescribed value i, then the cost is the same as for the planar case, and just as in the optimal modes P and AP, the plane change is free of additional fuel consumption. If the maximum plane change is less than the required plane change, the discussion is more subtle since the total plane change must be optimally distributed between the spatial phase and the atmospheric phase. This will be discussed in detail in Section 5.

Figure 5 shows the different regions of optimality for the case of $i = 50°$. As can be seen in the figures both the H set and the AE set are regressive as the plane change increases. When $i = 60.185°$, the Hohmann set disappears.

4. OPTIMAL ATMOSPHERIC TURNING

For a smooth transition from atmospheric flight to flight in the vacuum, it is convenient to use the modified Chapman's variables[7]

$$Z = \frac{\rho A C_{L^*}}{2m}\sqrt{\frac{r}{\beta}}, \qquad u = \frac{V^2}{gr} = \frac{V^2}{\mu/r} \tag{16}$$

to represent the altitude and the speed variable, and the dimensionless arc length

$$s = \int_0^t \frac{V}{r}\cos\gamma\, dt \tag{17}$$

to replace the time as the independent variable. The drag polar used is the parabolic drag polar

$$C_D = C_{D_0} + K C_L^2 \tag{18}$$

with the condition at maximum lift-to-drag ratio

$$\begin{aligned} C_L &= C_{L^*} = \sqrt{C_{D_0}/K}, \\ C_D &= C_{D^*} = 2C_{D_0}, \\ E^* &= C_{L^*}/C_{D^*}. \end{aligned} \tag{19}$$

Then, if σ is the bank angle, atmospheric turning can be achieved through the modulation of the vertical and the lateral component of the normalized lift coefficient

$$C = \frac{C_L}{C_{L^*}}\cos\sigma, \qquad S = \frac{C_L}{C_{L^*}}\sin\sigma. \tag{20}$$

With a Newtonian gravitational field, and a locally

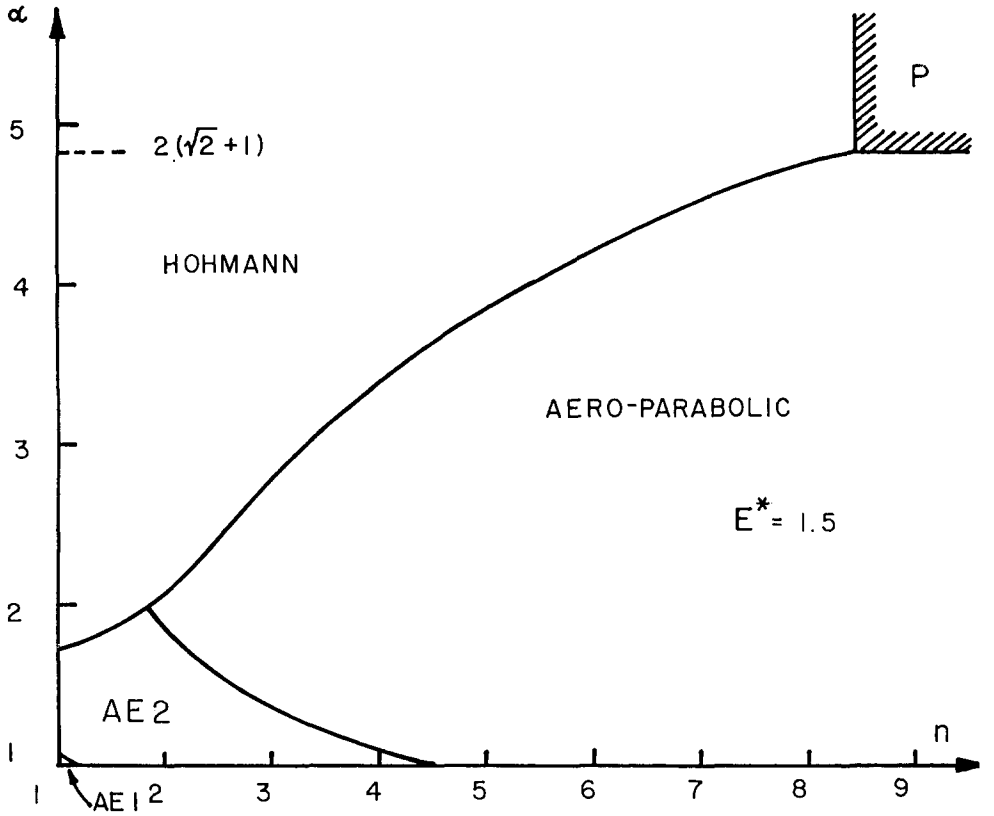

Fig. 4. Regions of optimality for $i = 30°$.

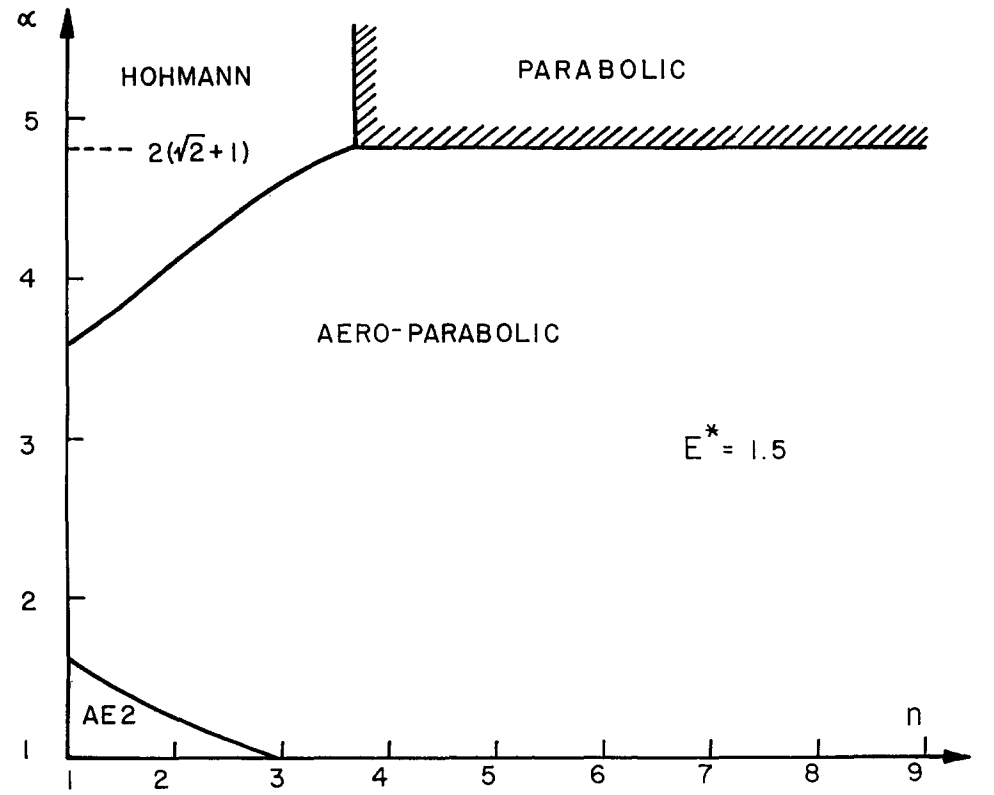

Fig. 5. Regions of optimality for $i = 50°$.

exponential atmosphere, and with the spherical coordinates as shown in Fig. 6, we have the universal dimensionless equations of motion

$$\begin{aligned}
\frac{dZ}{ds} &= -k^2 Z \tan\gamma \\
\frac{du}{ds} &= -\frac{kZu(1 + C^2 + S^2)}{E^* \cos\gamma} - (2 - u)\tan\gamma \\
\frac{d\gamma}{ds} &= \frac{k Z C}{\cos\gamma} + 1 - \frac{1}{u} \\
\frac{d\theta}{ds} &= \frac{\cos\psi}{\cos\phi} \\
\frac{d\phi}{ds} &= \sin\psi \\
\frac{d\psi}{ds} &= \frac{k Z S}{\cos^2\gamma} - \cos\psi\tan\phi.
\end{aligned} \tag{21}$$

In these equations, the only physical characteristic of the OTV is its maximum lift-to-drag ratio, E^*, and the nature of the atmosphere is specified by the constant value $k^2 = \beta r$, called Chapman's atmospheric parameter. For Earth's atmosphere, we take the value $k^2 = 900$, and for the OTV, we consider the case $E^* = 1.5$ for the computation.

Introducing the adjoint variables p_x, we form the Hamiltonian

$$\begin{aligned}
\mathrm{H} = {} & -k^2 Z p_Z \tan\gamma \\
& - p_u\left[\frac{kZu(1 + C^2 + S^2)}{E^* \cos\gamma} + (2 - u)\tan\gamma\right] \\
& + p_\gamma\left[\frac{kZC}{\cos\gamma} + 1 - \frac{1}{u}\right] \\
& + p_\theta \frac{\cos\psi}{\cos\phi} + p_\phi \sin\psi \\
& + p_\psi\left[\frac{kZS}{\cos^2\gamma} - \cos\psi\tan\phi\right].
\end{aligned} \tag{22}$$

The maximization of the Hamiltonian with respect to the controls C and S leads to the optimal law

$$C = \frac{E^* p_\gamma}{2u p_u}, \qquad S = \frac{E^* p_\psi}{2u p_u \cos\gamma}. \tag{23}$$

Along the optimal trajectory, the adjoint component p_x, for any variable x, satisfies the adjoint equation

$$\frac{dp_x}{ds} = -\frac{\partial \mathrm{H}}{\partial x}. \tag{24}$$

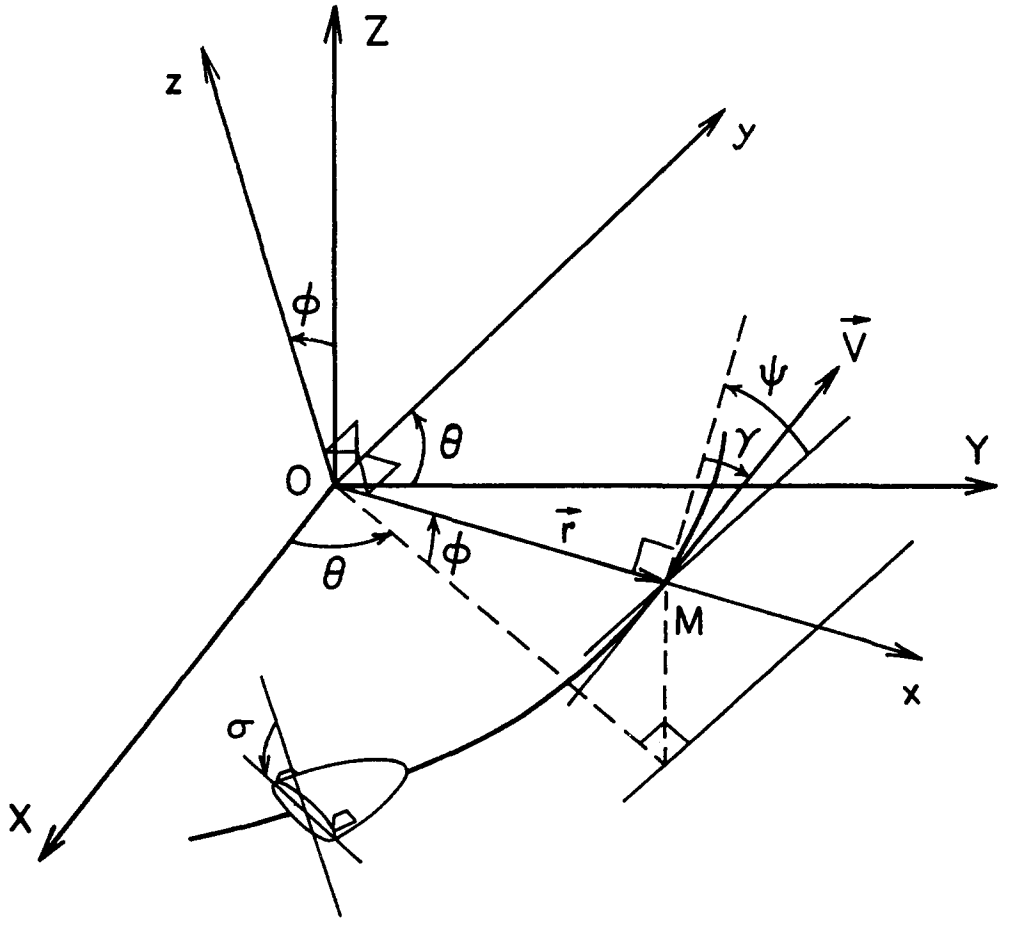

Fig. 6. Spherical coordinates for atmospheric flight.

It is known that the problem has the following integrals[2]

$$\begin{aligned} &H = c_0,\ p_\theta = c_1,\ p_\phi = c_2 \sin\theta - c_3 \cos\theta \\ &p_\psi = c_1 \sin\phi + (c_2 \cos\theta + c_3 \sin\theta)\cos\phi, \end{aligned} \tag{25}$$

where the c_i are constants of integration. In this problem of optimal turning, we are concerned with speed depletion and heading change without prescribing the final arc length s_f and final longitude θ_f. Hence, by the transversality condition

$$c_0 = 0, \qquad c_1 = 0. \tag{26}$$

With four integrals, only two of the remaining adjoint equations need be integrated. Their integration requires guessing two initial values which, together with c_2 and c_3, constitute a four-parameter problem. By normalizing the adjoint variables, we are led to a three-parameter problem.

The difficulty in estimating these parameters can be alleviated by using the controls C and S, as given in eqns (23), to replace the adjoints. By taking the derivatives of these equations, using the equations for the adjoints according to the optimality condition (24), we have directly the equations for the control

$$\begin{aligned} \frac{dC}{ds} = \frac{2C}{E^*u}(C + E^* \tan\gamma) + \frac{1}{\cos^2\gamma}\Bigg[k^2F \\ + \frac{E^*(2-u)}{2u} + \frac{kZ}{2}(1 - C^2 - 3S^2)\sin\gamma\Bigg], \end{aligned} \tag{27}$$

and

$$\begin{aligned} \frac{dS}{ds} = \frac{2SC}{E^*u} + S\tan\gamma\left(\frac{kZC}{\cos\gamma} + 1 + \frac{1}{u}\right) \\ - S\tan\phi\sin\psi - \frac{G\cos\psi}{\cos\gamma}, \end{aligned} \tag{28}$$

where F and G are defined as the ratios

$$F = \frac{E^*Zp_Z}{2u\,p_u}, \qquad G = \frac{E^*p_\phi}{2u\,p_u}. \tag{29}$$

The equations for F and G can also be easily obtained as

$$\begin{aligned} \frac{dF}{ds} = \frac{2F}{E^*u}(C + E^*\tan\gamma) \\ + \frac{kZ}{2\cos\gamma}(1 - C^2 - S^2) \end{aligned} \tag{30}$$

and

$$\begin{aligned} \frac{dG}{ds} = \frac{2G}{E^*u}(C + E^*\tan\gamma) \\ + \frac{S}{\cos^2\phi}\cos\gamma\cos\psi. \end{aligned} \tag{31}$$

In summary, besides the six state equations (21), we have four equations providing directly the controls C and S and the accessory variables F and G. Their integration requires guessing only three initial parameters C_e, S_e and G_e at the initial entry time, while F_e can be computed from the Hamiltonian integral, with $c_0 = c_1 = 0$:

$$\begin{aligned} -k^2F\tan\gamma - \frac{E^*(2-u)}{2u}\tan\gamma \\ - \frac{kZ}{2\cos\gamma}(1 - C^2 - S^2) \\ - S\cos\gamma\cos\psi\tan\phi + C\left(1 - \frac{1}{u}\right) \\ + G\sin\psi = 0. \end{aligned} \tag{32}$$

As a matter of fact, because of this relation, we can delete one of the differential equations.

4.1 *Transversality conditions*

At the initial time, $s_e = 0$, we have the values of the state variables

$$\begin{aligned} &\theta_e = \phi_e = \psi_e = 0, \\ &Z_e = 0.0002, \\ &\gamma_e,\ u_e \text{ prescribed}. \end{aligned} \tag{33}$$

The value Z_e has been selected so that for a typical OTV, the atmospheric force is slightly felt to have a small but detectable effect on the incoming Keplerian trajectory. The initial angle γ_e is very small, of a few degrees, and is just sufficient for the required plane change to be accomplished. The initial value of u_e is computed when the descending trajectory for atmospheric entry has been specified.

It is proposed, for a prescribed speed depletion, to maximize the plane change i, that is the function

$$J = -\cos i_f = -\cos\phi_f\cos\psi_f. \tag{34}$$

At the final, exit point, we have

$$Z_f = Z_e, \qquad u_f = \text{prescribed}, \qquad \gamma_f = \text{free}. \tag{35}$$

We have the transversality conditions

$$\begin{aligned} P_{\phi_f} &= \frac{\partial J}{\partial\phi_f} = \sin\phi_f\cos\psi_f \\ P_{\psi_f} &= \frac{\partial J}{\partial\psi_f} = \cos\phi_f\sin\psi_f \\ P_{\gamma_f} &= \frac{\partial J}{\partial\gamma_f} = 0. \end{aligned} \tag{36}$$

From the eqns (23) and (29), these are expressed as

$$C_f = 0, \qquad \frac{G_f}{S_f} = \frac{\tan\phi_f\cos\gamma_f}{\tan\psi_f}. \tag{37}$$

In summary, to search for the optimal trajectory, we must guess the initial values C_e, S_e and G_e while computing F_e from the Hamiltonian integral (32). At the final

altitude $Z_f = Z_e$, used as stopping condition, the condition of u_f and the two transversality conditions (37) are used for matching. Since C_e and S_e have physical meaning, and for small lateral range G remains small, the correct guessing is relatively easy.

4.2 *Numerical Results*

The solutions have been generated for several values of $u_e = V_e^2/(\mu/R)$, and the results are presented in Fig. 7. In this figure we have plotted $\sqrt{u_f} = V_f/\sqrt{\mu/R}$ vs u_e, using the plane change i as parameter. The plot gives the complete graphical solution for the case of $E^* = 1.5$ ranging from circular entry, $u_e = 1$, to parabolic entry, $u_e = 2$, and for plane change from 0° to 60°. For example, taking $u_e = 1.25$, that is an entry speed $V_e = 1.118\ V_c$ where V_c is the circular speed at distance R, a reduction to circular speed, $u_f = 1$, will provide a maximum plane change of just over $i = 9°$. If a 23° plane change is desired, the final speed is $V_f = 0.837\ V_c$.

Figures 8 to 11 show the behavior of the state and control variables for two typical optimal turning trajectories, one leading to supercircular speed exit, $u_f > 1$, shown in dashed lines, and the other leading to subcircular speed exit, $u_f < 1$, shown in solid lines. In both cases, the entry speed variable is $u_e = 1.733$, and this corresponds to entry speed for a direct return from GEO. The plane change obtained in the first case is 20°.9 and for the second case, it is increased to 42°.9. The abscissas in the figures are the longitudes. Figure 8 shows the variations of the speed $\sqrt{u} = V/\sqrt{gr}$, and the altitude from the entry point. From definition (16), we have the linear change in the altitude

$$\beta\Delta h = \log (Z/Z_e). \tag{38}$$

It is seen that for large plane change, the trajectory gets deeper in the dense atmosphere for turning. It is also there that the most speed depletion occurs. It is obvious that most of the plane change occurs while the OTV is at low altitude as shown in Fig. 9 for the change in the heading. At the beginning and at the end of the trajectory, the heading is near stationary and the variation in the latitude is linear. Figure 10 shows the variations of the flight path angle. For supercircular exit, the exit angle is approximately $\gamma_f \approx -1/2\ \gamma_e$, while for subcircular exit it is nearly zero. Finally, Fig. 11 shows the variations of the normalized lift coefficient $\lambda = C_L/C_{L^*}$. As seen in the figure, it is near the value $\lambda = 1$ for maximum lift-to-drag ratio. For the bank angle plotted in the same figure, as shown in the rear view sketch of the vehicle, when σ exceeds 90° the lift force is pointing downward. This occurs at the beginning of the trajectory for a quick descent to low altitude for turning. Because of the transversality condition $C_f = 0$, the final bank angle is $\sigma_f = 90°$. For high speed exit, the second half of the trajectory is flown with practically no vertical lift component. The OTV skips out based on the strength of the speed, in ballistic mode. Vertical positive lift component is required in the second half of the trajectory for subcircular speed exit. Because of this lift component, it is possible to control the flight path angle for grazing exit, $\gamma_f = 0$. The computation of the normalized lift coefficient and the bank angle is based on the definition (20), explicited as

$$\lambda = \frac{C_L}{C_{L^*}} = \sqrt{C^2 + S^2},\ \tan\sigma = \frac{S}{C}. \tag{39}$$

5. SOLUTION TO THE AEROASSISTED-ELLIPTIC MODE

We are now in the position to analyze this lifting mode. As discussed in Section 3, this is the only mode that requires the splitting of the plane change angle between

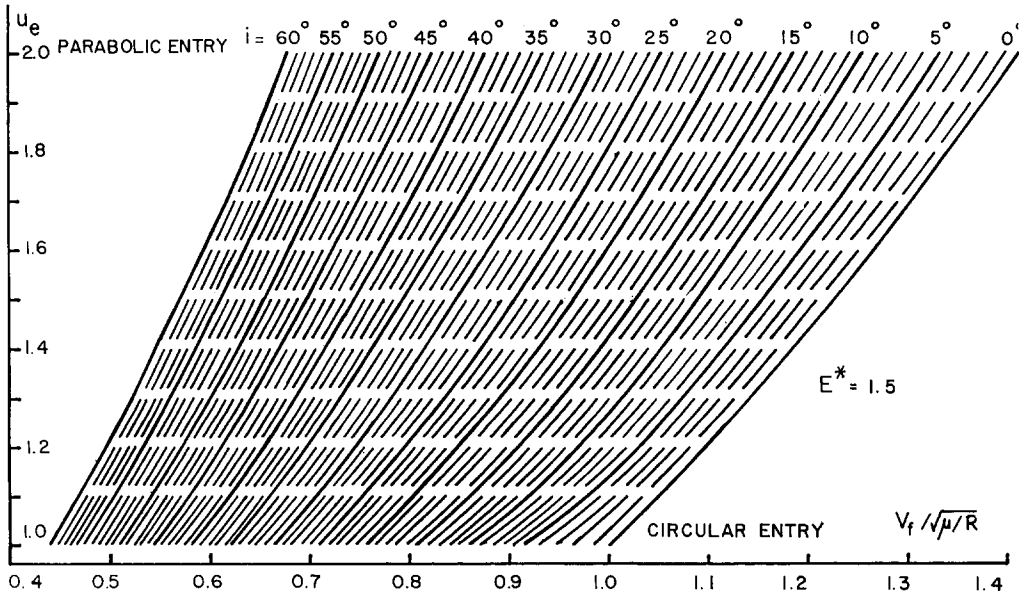

Fig. 7. Maximum plane change for prescribed speed depletion.

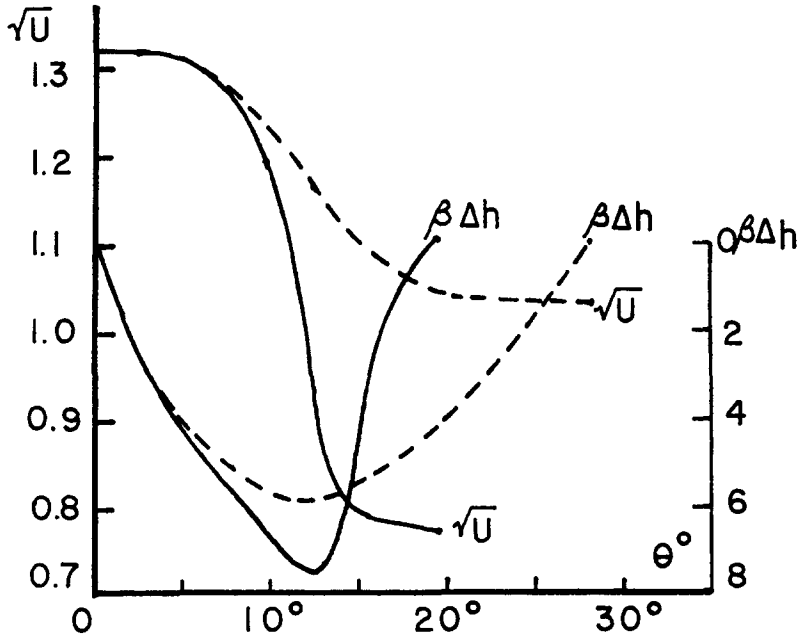

Fig. 8. Variations of altitude and speed.

the space phase and the atmospheric phase. The general problem is to find the optimal mode and compute its solution for given n, a and i. As an example, we consider the case of $n = 2$, $a = 1.04$ and $i = 30°$. With $R = 6498$ km, for an entry altitude of $h_e = 120$ km, this corresponds to a LEO at an altitude of 380 km. With this value of a, the P mode is nonoptimal. A quick check of Fig. 4 rules out the H mode in favor of the AP mode. More precisely, for the H mode, we use the explicit solution in Section 3 to obtain the limiting value $i = 36°.165$ for the three-impulse to become optimal. A check of Fig. 3 confirms this assessment. For the optimal

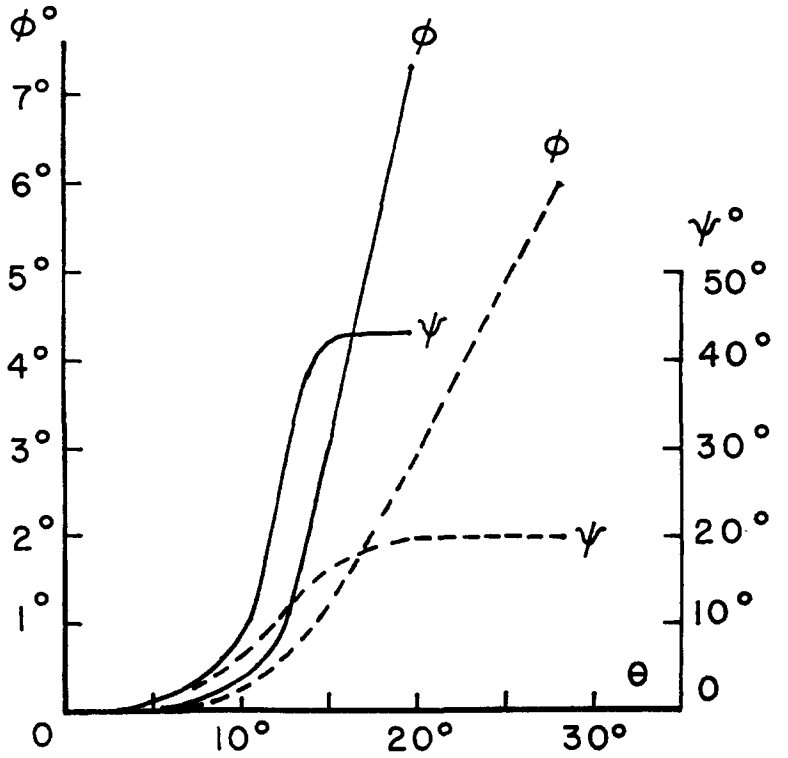

Fig. 9. Variations of latitude and heading.

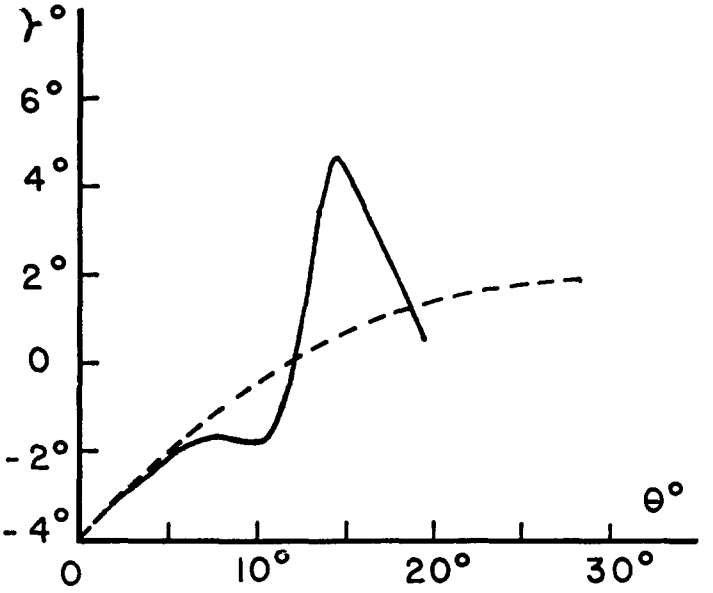

Fig. 10. Variations of flight path angle.

two-impulse pure propulsive transfer, we obtain

$$\Delta v_H = 0.486390, \tag{40}$$

while for the AP mode, from eqn (6)

$$\Delta v_{AP} = 0.302746. \tag{41}$$

It remains to be seen that, as shown in Fig. 4, the AE mode with two-impulse deorbit is truly optimal.

First, the following nonoptimal scheme as generally accepted in the published literature is considered: a one-impulse planar deorbit for an entry angle γ_e, followed by atmospheric plane change of the required amount with a second impulse at exit for ascent and circularization at LEO by a third impulse.

With $a_1 = na$, and using circular speed at LEO as

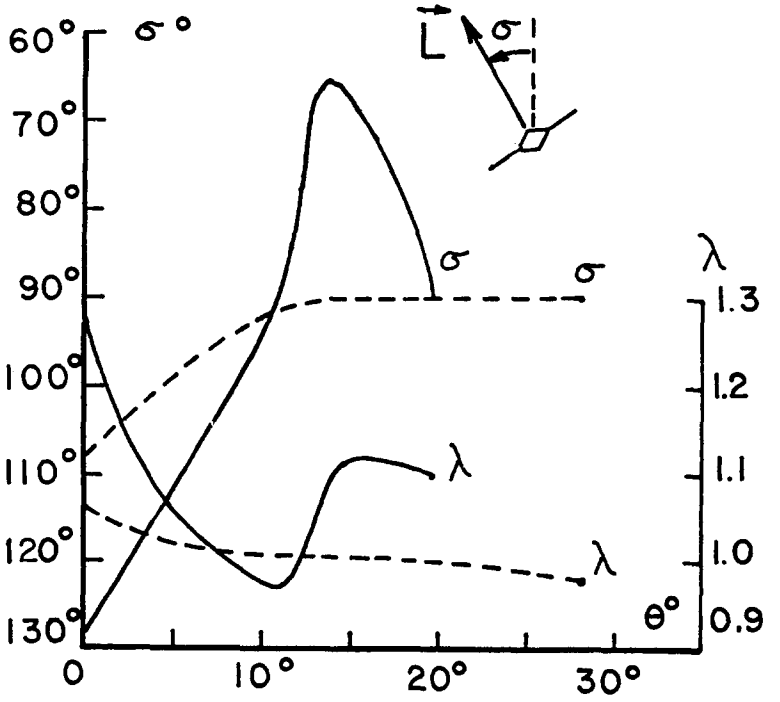

Fig. 11. Variations of lift and bank.

unit speed, the characteristic velocity for deorbit is

$$\Delta v_1 = \frac{1}{\sqrt{n}}\left[1 - \sqrt{\frac{2(a_1 - 1)}{a_1^2 - \cos^2\gamma_e}}\cos\gamma_e\right]. \quad (42)$$

We also have the value for the entry speed variable

$$u_e = \frac{2a_1(a_1 - 1)}{a_1^2 - \cos^2\gamma_e}. \quad (43)$$

To achieve a plane change of 30°, an entry angle near $\gamma_e = -3°$ must be selected. The equations for optimal turning in Section 4 can be used with the same transversality conditions (37) since the problem is now viewed as maximizing the exit speed with a prescribed plane change. At exit, we have $u_f = 0.636873$, $\gamma_f = 0$. To reach LEO at apogee, a second impulse is applied tangentially at exit. Its magnitude is

$$\Delta v_2 = a\sqrt{\frac{2(a - 1)}{a^2 - \cos^2\gamma_f}} - \sqrt{au_f}. \quad (44)$$

At apogee, the third and final impulse required for circularization is

$$\Delta v_f = 1 - \sqrt{\frac{2(a - 1)}{a^2 - \cos^2\gamma_f}}\cos\gamma_f. \quad (45)$$

The total characteristic velocity of this nonoptimal mode is found to be

$$\Delta v = 0.364077. \quad (46)$$

Hence, although there is fuel saving as compared to the Hohmann mode, which is the best pure propulsive mode, the fuel consumption is still higher than that for the AP mode.

As an improvement toward obtaining the best solution, a preliminary numerical study shows that in this region, any attempt to add more atmospheric plane change, called forced plane change, at the expense of reducing the value u_f to be less than the necessary value for climbing to LEO, will lead to higher fuel consumption. Hence, the optimal condition is that $\Delta v_2 = 0$, and from eqn (44), we have

$$u_f = \frac{2a(a - 1)}{a^2 - \cos^2\gamma_f}. \quad (47)$$

If the exit condition satisfies this relation, then in postatmospheric flight, the only impulse required is the last impulse as given in eqn (45). In this case, the atmospheric plane change is called free plane change since we have optimally used the required speed depletion for plane change.

If we use one single impulse for deorbit while also making a plane change i_1, then the entry value u_e is still as given in eqn (43), but due to the plane change, the characteristic velocity for deorbit is now

$$\Delta v_1 = \frac{1}{\sqrt{n}}\left[\frac{a_1^2 + (2a_1 - 3)\cos^2\gamma_e}{\alpha_1^2 - \cos^2\gamma_e} - 2\cos\gamma_e\cos i_1\sqrt{\frac{2(a_1 - 1)}{a_1^2 - \cos^2\gamma_e}}\right]^{1/2}. \quad (48)$$

With a small entry angle γ_e selected, just enough for completing the atmospheric turning leading to condition (47), the maximized free atmospheric plane change i_a can be computed. To compute the space plane change i_1, we refer to Fig. 12 where $\mathbf{h}_1$ is the unit angular momentum orthogonal to the plane of the first orbit. If OX is the line of apsides, after deorbit $\mathbf{h}_1$ becomes $\mathbf{h}$ orthogonal to the plane of the entry trajectory after rotating by the angle i_1 in the YZ plane. After atmospheric plane change by the angle i_a, it becomes $\mathbf{h}_f$ orthogonal to the plane of the final orbit. If Ω_f is the longitude of the ascending node of the final plane, we have $\mathbf{h}_1 = (0, \sin i_1, \cos i_1)$ and $\mathbf{h}_f = (\sin i_a \sin\Omega_f, -\sin i_a \cos\Omega_f, \cos i_a)$. Hence, we have the relation

$$\mathbf{h}_1 \cdot \mathbf{h}_f = \cos i = \cos i_1 \cos i_a - \cos\Omega_f \sin i_1 \sin i_a. \quad (49)$$

Because of the effect of nonzero entry angle, entry starts behind the X-axis by an angle ω such that

$$\sin\omega = -\frac{2a_1(a_1 - 1)\sin\gamma_e\cos\gamma_e}{a_1^2 - (2a_1 - 1)\cos^2\gamma_e}. \quad (50)$$

After evaluating this angle, we can compute Ω_f from

$$\sin\psi_f = \sin i_a \cos[\theta_f - (\omega + \Omega_f)], \quad (51)$$

where the longitude θ_f in atmospheric flight is measured from the OX_e axis passing through the entry point. Because of the spherical trigonometry relations (49) and (51), the initial plane change i_1 is slightly higher than the complement $i - i_a$.

If this AE mode with one-impulse deorbit is followed, we have $\gamma_e = -3°$, $u_e = 1.349538$ from eqn (43), and $\omega = 11°.527$ from eqn (50). The free atmospheric plane change provides $i_a = 12°.107$ with the elements at exit being $\theta_f = 34°.942$, $\phi_f = 4°.291$, $\gamma_f = 1°.177$, $u_f = 1.014363$ and $\psi_f = 11°.332$. Thus $\Omega_f = 2°.945$ and the preliminary plane change is $i_1 = 17°.903$ from eqn (49). The total characteristic velocity for this maneuver is

$$\Delta v = 0.253613, \quad (52)$$

which shows a net improvement over the forced atmospheric plane change as given in eqn (46). Furthermore, this mode is now seen as better than the AP mode.

Finally, it is a simple exercise to show that under the present situation, to deorbit for an entry angle $\gamma_e = -3°$ while achieving a propulsive plane change $i_p = 17.903°$, a two-impulse scheme is better than the one-impulse mode. For a two-impulse deorbit, the first impulse is applied orthogonally to the position vector at HEO, to

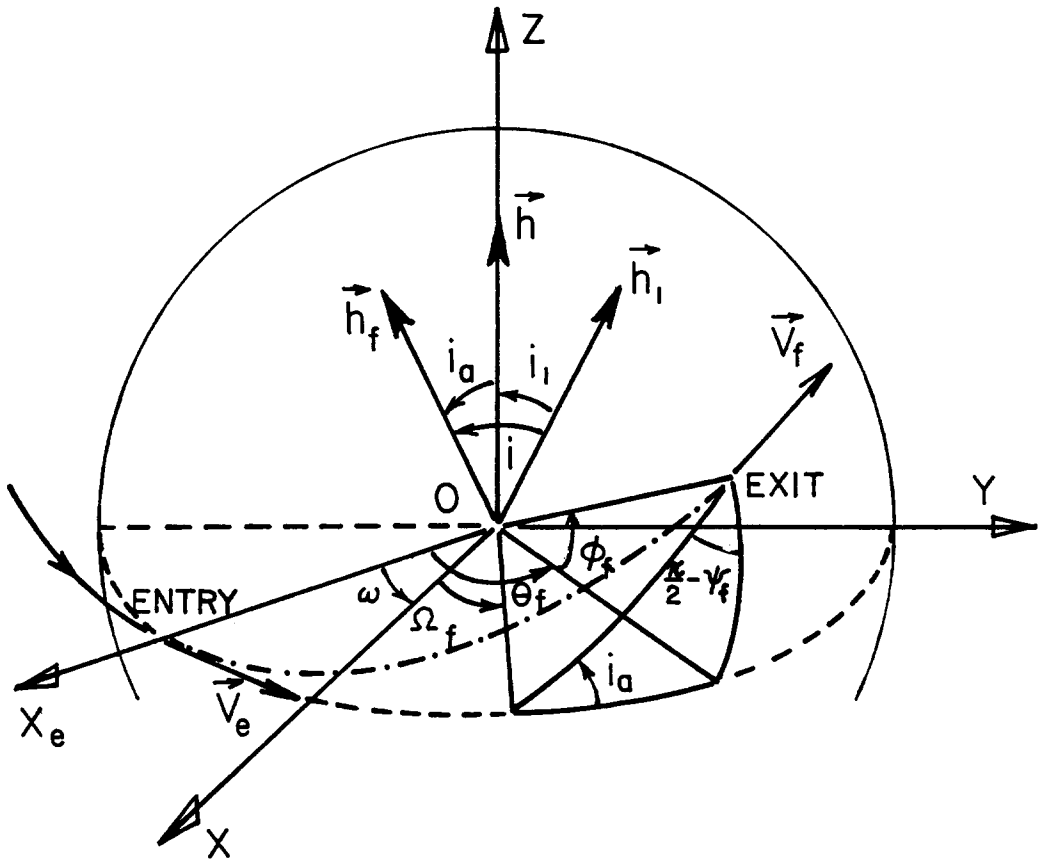

Fig. 12. Geometry of plane change.

propel the OTV into a higher elliptic orbit reaching an apogee at a distance $r_1 x$ while making a plane change i_1. The required characteristic velocity is

$$\Delta v_1 = \left[\frac{1}{n}\left(\frac{3x+1}{x+1} - 2\sqrt{\frac{2x}{x+1}}\cos i_1\right)\right]^{1/2}. \quad (53)$$

At this apogee, a second orthogonal impulse is applied to return the vehicle for reentry at the prescribed angle γ_e while making the remaining propulsive plane change $i_2 = i_p - i_1$. The required characteristic velocity is

$$\Delta v_2 = \left[\frac{2}{nx} \times \left[\frac{a_1^2x^2 + (a_1x^2 + a_1x - x - 2)\cos^2\gamma_e}{(x+1)(a_1^2x^2 - \cos^2 a_e)} - 2\sqrt{\frac{(a_1x-1)}{(x+1)(a_1^2x^2-\cos^2\gamma_e)}} \times \cos\gamma_e \cos(i_p - i_1)\right]\right]^{1/2}. \quad (54)$$

For a given i_p, the minimization of the sum $\Delta v_1 + \Delta v_2$ with respect to x and i_1 leads to the conditions for optimal two-impulse deorbit. But, it should be noticed that by going out to a larger distance, $x > 1$, the entry speed is now higher as computed from

$$u_e = \frac{2a_1 x(a_1x - 1)}{a_1^2 x^2 - \cos^2\gamma_e}. \quad (55)$$

As a consequence, the free atmospheric plane change i_a is also higher, thus reducing the propulsive plane change i_p. In other words, there is coupling between space and atmospheric maneuver. To solve this problem, for each value of x, we minimize the sum $\Delta v_1 + \Delta v_2$ with respect to i_1 to have

$$\sin i_1 = \frac{\Delta v_1}{\Delta v_2}\sqrt{\frac{2(a_1x-1)}{x^3(a_1^2x^2 - \cos^2\gamma_e)}} \times \cos\gamma_e \sin(i_p - i_1). \quad (56)$$

This gives the optimal condition for splitting the propulsive plane change i_p. By changing i_1 into i_p in eqn (49) we have the equation for the total plane change in the case of two-impulse deorbit. The longitude of the ascending node Ω_f is still given by eqn (51) but now the angle ω is obtained from

$$\sin\omega = -\frac{2a_1x(a_1x-1)\sin\gamma_e\cos\gamma_e}{a_1^2x^2 - (2a_1x-1)\cos^2\gamma_e}. \quad (57)$$

Using x as parameter for optimization, we can compute u_e and the optimal atmospheric plane change i_a, and then the total propulsive plane change i_p as for the one-impulse case. The condition (56) gives the optimal split between i_1 and i_2. The total cost for the transfer is the sum $\Delta v_1 + \Delta v_2 + \Delta v_f$. In this way, we can search for the optimal value of x. The computation has been done, and now with higher entry speed, it requires the entry

angle $\gamma_e = -3°.5$ with the optimal value $x = 1.463$ providing $u_e = 1.504644$. With these values of entry angle and entry speed the optimal atmospheric turning starts with $C_e = -0.24383$, $S_e = 1.01008617$, and $G_e = -0.243883$. The end results are $i_a = 16°.765$, $\theta_f = 32°.965$, $\psi_f = 15°.791$, $\gamma_f = 1°.294$ and $u_f = 1.01327$. This gives $\omega = 10°.411$, $\Omega_f = 3°.189$ and $i_p = 13°.246$. This angle splits into $i_1 = 2°.059$, $i_2 = 11°.187$ with the total characteristic velocity

$$\Delta v_{\text{opt}} = 0.22969. \tag{58}$$

A refined calculation shows that, for an absolute optimal solution, there is a very small plane change at the last impulse.

We notice that the effect of nonzero entry angle γ_e and exit angle γ_f on performance computation is small since by adding linearly the plane changes we have 30°.01, and if zero entry and exit angle are used, the cost was determined as 0.22625. This leads us to devise a computer program for a preliminary computation of the AE mode.

First, the optimal atmospheric problem is solved for five values of u_e ranging from circular entry, $u_e = 1$, to parabolic entry, $u_e = 2$, leading to plane change from 0° to 60° in increments of 1°, with resulting final speed u_f. The results were stored in a data file. Figure 7 represents a graphical display of the solution. For any value of u_e, and atmospheric plane change i_a, cubic splines are used to obtain u_f. For fractions of a degree, linear interpolation was used. With this, the global optimal problem becomes a parametric optimization problem.

The preatmospheric maneuver is propulsive with one or two impulses. By going out a distance $r_1 x$, with grazing entry, $\gamma_e = 0$, the entry speed is

$$u_e = \frac{2a_1 x}{a_1 x + 1}. \tag{59}$$

With plane changes i_1 and i_2 at the impulses, we have the characteristic velocities

$$\Delta v_1 = \left[\frac{1}{n}\left(\frac{3x+1}{x+1} - 2\sqrt{\frac{2x}{x+1}}\cos i_1\right)\right]^{1/2} \tag{60}$$

and

$$\Delta v_2 = \left\{\frac{2}{nx}\left[\frac{(a_1 x + x + 2)}{(x+1)(a_1 x+1)} - \frac{2\cos i_2}{\sqrt{(x+1)(a_1 x+1)}}\right]\right\}^{1/2}. \tag{61}$$

Similarly, for the propulsive postatmospheric maneuver, at exit angle $\gamma_f = 0$, and exit speed u_f, we consider the general case where a possible Δv_3 with plane change i_3 is required immediately at exit to boost the vehicle to LEO for circularization by a Δv_4 with plane change i_4. The characteristic velocities are respectively

$$\Delta v_3 = \left[\frac{a(a+1)u_f + 2a^2}{a+1} - 2a\sqrt{\frac{2au_f}{a+1}}\cos i_3\right]^{1/2} \tag{62}$$

and

$$\Delta v_4 = \left[\frac{a+3}{a+1} - 2\sqrt{\frac{2}{a+1}}\cos i_4\right]^{1/2}. \tag{63}$$

If i_p is the total propulsive plane change, we have the constraint

$$i_1 + i_2 + i_3 + i_4 - i_p = 0. \tag{64}$$

By selecting a value x, we choose the entry speed $u_e(x)$. By selecting a value for the atmospheric plane change i_a, we choose the exit speed $u_f(i_a)$. Hence, x and i_a, or equivalently u_e and u_f, are the ultimate parameters for optimization. With i_a selected, we have the value $i_p = i - i_a$. For each pair of values x and i_a, the optimal distribution of the propulsive plane changes is obtained by introducing the Lagrange multiplier q to handle the constraint (64) and by minimizing the augmented function

$$J = \sum_{i=1}^{4} \Delta v_i + q(i_1 + i_2 + i_3 + i_4 - i_p). \tag{65}$$

We have then the necessary conditions

$$\sqrt{\frac{2x}{x+1}}\sin i_1 = -nq\,\Delta v_1 \tag{66}$$

$$\frac{2\sin i_2}{x\sqrt{(x+1)(a_1 x+1)}} = -nq\,\Delta v_2 \tag{67}$$

$$a\sqrt{\frac{2au_f}{a+1}}\sin i_3 = -q\,\Delta v_3 \tag{68}$$

$$\sqrt{\frac{2}{a+1}}\sin i_4 = -q\,\Delta v_4. \tag{69}$$

For each x and i_a, the eqns (66)–(69), together with the constraint (64), are solved for the propulsive plane changes, and subsequently, by iteration on x and i_a, the optimal solution is obtained.

For a given triplet (n, a, i), the program first searches for the no-extra-cost atmospheric plane change with $i_p = 0$. With this, we have $i_1 = 0$, $\Delta v_1 = 0$, $x = 1$;

that is, the first impulse is inoperative. The planar deorbit is by one impulse which is here represented by Δv_2. The entry speed is given by eqn (59) with $x = 1$. With $i_3 = 0$, $\Delta v_3 = 0$, and from eqn (62), we have the exit speed. Hence, we obtain

$$u_e = \frac{2a_1}{a_1 + 1}, \qquad u_f = \frac{2a}{a + 1}. \tag{70}$$

These conditions provide the maximum atmospheric plane change i_{a^*} with the same cost as for planar return. If the prescribed i is less than this value, we simply waste more energy during atmospheric flight. It is only in the case where $i > i_{a^*}$ that we have plane change in the propulsive mode, $i_p \neq 0$. But in this case, not all the propulsive plane changes are always present.

First, as noticed above, we have the case of optimal one-impulse deorbit, denoted by AE1. The first impulse is inoperative and $i_1 = 0, x = 1$. For $i_p \neq 0$, the plane change i_2 never vanishes since for $i_2 = 0$, with $q \neq 0$, to satisfy condition (67), we have $\Delta v_2 = 0$, which leads to $(a_1 - 1)^2 x^2 = 0$ and hence the case where $a_1 = 1$. For the case AE1, we have two possibilities in postatmospheric flight. First, with $i_3 = 0$, $\Delta v_3 = 0$, the exit speed is as given in eqn (70), just necessary for a climb to LEO. We have the case of free atmospheric plane change, and only one impulse is required for circularization with plane change i_4. By eqns (63) and (69), $i_4 = 0$ only in the limiting case where $a = 1$. Next, we have the case where $i_3 \neq 0$, and the value u_f is less than the one given in eqn (70). This is the case of forced atmospheric plane change, and two impulses are required in postatmospheric flight. The mode AE1 occurs for small values of i and/or near the origin, $n \approx 1$, $a \approx 1$, as shown in Fig. 4.

As shown in Figs. 4 and 5, we have mainly the case of two-impulse deorbit, denoted by AE2. Because of high entry speed, this mode leads to $i_3 = 0$, hence to free atmospheric plane change. Two impulses are required for deorbit and one last impulse is necessary for circularization. Plane change occurs whenever an impulse is applied although the last plane change i_4 is generally small because the AE mode is optimal for low LEO. For that reason, in the complete example above, we have set both $i_3 = 0$, $i_4 = 0$, for the sake of clarity in the discussion.

This program, with the approximation $\gamma_e = 0$, $\gamma_f = 0$, has been used to find the regions of optimality in the section i = constant as depicted in Figs. 4 and 5. In between these figures, when $i \approx 40°3$ the point where the three modes H, AP and AE are equal occurs on the $n = 1$ axis, at the point $a \approx 2.39$. Then, beyond Fig. 5, the AE mode disappears when i reaches the value of about 59°. Finally, as mentioned above, the H mode disappears when $i = 60°185$.

6. CONCLUSION

This paper gives a complete analysis of the problem of aeroassisted return from a high Earth orbit to a low Earth orbit with plane change. A discussion of pure propulsive maneuver leads to the necessary change for improvement of the fuel consumption by inserting in the middle of the trajectory an atmospheric phase to obtain all or part of the required plane change. The variational problem is reduced to a parametric optimization problem by using the known results in optimal impulsive transfer, and solving the atmospheric turning problem for storage and use in the optimization process. The coupling effect between space maneuver and atmospheric maneuver is discussed. Depending on the values of the plane change i, the ratios of the radii, $n = r_1/r_2$ and $a = r_2/R$ and the maximum lift-to-drag ratio E^*, the optimal maneuver can be pure propulsive or aeroassisted. For aeroassisted maneuver, the optimal mode can be parabolic, which only requires drag capability of the vehicle, or elliptic. In the elliptic mode, it can be one-impulse for deorbit and one- or two-impulse in postatmospheric flight, or by two-impulse for deorbit with only one-impulse for final circularization. It is shown that whenever an impulse is applied, a plane change is made. The necessary conditions for the optimal split of the plane changes are derived and mechanized in a computer program for the solution.

Acknowledgment—This work was supported in part by the Jet Propulsion Laboratory under contract No. 956416 with Dr. K. D. Mease as the technical monitor.

REFERENCES

1. H. S. London, Change of satellite orbit plane by aerodynamic maneuvering. *JAS* **29**, 323–332 (1962).
2. N. X. Vinh, *Optimal Trajectories in Atmospheric Flight*. Elsevier Scientific Publishing Co., Amsterdam and New York (1981).
3. G. D. Walberg, A review of aeroassisted orbit transfer. AIAA paper No. 82-1378, AIAA 9th Atmospheric Flight Mechanics Conference, San Diego, California (1982).
4. M. I. Cruz *et al.*, Optimization and closed-loop guidance of drag modulated aeroassisted orbital transfer. AIAA paper No. 83-2093, AIAA 10th Atmospheric Flight Mechanics Conference, Gatlinburg, Tennessee (1983).
5. C. Marchal, Transferts optimaux entre orbites elliptiques (durée indifférente). Doctoral thesis, AO 1609 Paris (1967).
6. J. P. Marec, *Optimal Space Trajectories*. Elsevier Scientific Publishing Co., Amsterdam and New York (1979).
7. J. S. Chern and N. X. Vinh, Optimum reentry trajectories of a lifting vehicle. NASA CR-3236 (1980).